Catalysis Science & Technology

ROYAL SOCIETY OF CHEMISTRY

PAPER

Cite this: *Catal. Sci. Technol.*, 2021, 11, 4509

Surface reactions of ammonia on ruthenium nanoparticles revealed by ^{15}N and ^{13}C solid-state NMR†

Niels Rothermel,[a] Hans-Heinrich Limbach,[b] Iker del Rosal,[c] Romuald Poteau,*[c] Gabriel Mencia,[c] Bruno Chaudret,[c] Gerd Buntkowsky*[a] and Torsten Gutmann*[a]

Ruthenium nanoparticles (Ru NPs) stabilized by bis-diphenylphosphinobutane (dppb) and surface-saturated with hydrogen have been exposed to gaseous $^{15}NH_3$ and studied using solid-state ^{15}N CP MAS NMR. Three signals have been observed at 24.5, −12 and −42 ppm (reference external liquid ammonia) which are assigned to chemisorbed ammonia species $RuNH_x$. Sample exposure to vacuum or aging leads to conversion of the 24.5 ppm species into the other ones, a process which is reversed by re-exposure to hydrogen gas. Exposure to a mixture of $^{15}NH_3$ and ^{13}CO leads to the formation of surface bound urea as demonstrated by ^{15}N and ^{13}C CP MAS NMR. To understand the surface reactions of ammonia and the ^{15}N NMR results, quantum chemical calculations of the structures, energies and ^{15}N chemical shifts of ammonia species on Ru_6 and Ru_{55} model clusters have been performed. The calculations indicate that under the experimental conditions applied, the fractions of $RuNH_3$ and $RuNH_2$ species are similar, independent of the H_2 pressure. No RuN and RuNH species are formed which are calculated to resonate at a lower field than the signals observed experimentally. However, the ^{15}N chemical shifts of $RuNH_2$ depend on the number of neighboring surface hydrogens and hence on the H_2 pressure. Thus, the signal at 24.5 ppm is assigned to $RuNH_2$ in a neighborhood rich in surface hydrogens. $RuNH_2$ depleted in neighboring surface hydrogens and $RuNH_3$ resonated both in a similar chemical shift range to which the signals at −12 and −42 belong. A change of the hydrogen pressure then leads to interconversion of hydrogen-rich and hydrogen-poor neighborhoods of $RuNH_2$ but does not alter the fractions of $RuNH_3$ and $RuNH_2$ according to the calculated stability diagram. Nevertheless, dissociation of $RuNH_3$ into $RuNH_2$ and surface hydrogen is expected to take place during the initial ammonia adsorption process and at low H_2 pressures and high temperatures. Finally, some preliminary quantum chemical calculations suggest stepwise binding of two NH_2 groups to adsorbed CO leading to surface bound urea where the oxygen is coordinated to Ru.

Received 29th December 2020,
Accepted 24th April 2021

DOI: 10.1039/d0cy02476g

rsc.li/catalysis

Introduction

Ammonia is the main source of reactive nitrogen in the chemical industry. It is used for the production of platform chemicals such as nitric acid[1] and urea,[2] with widespread applications in today's manufacturing processes of fertilizers.[3] Moreover, ammonia is discussed as a key molecule in the formation of amino acids which are the basis for the genesis of life,[4–6] and in the synthesis of a variety of nitrogen containing organic compounds.[7]

With the pioneering work by Haber and Bosch, ammonia has become accessible directly from nitrogen.[8,9] In the subsequent time, the process of ammonia synthesis has been continuously optimized and a large variety of catalysts has been developed. With the advancement of analytical and computational techniques in the past decades, significant efforts have been made to understand the mechanism behind the ammonia production.[10–14] In this context, ruthenium containing catalysts have been found to be highly efficient.[15,16] In particular, supported ruthenium

[a] *Technical University of Darmstadt, Institute of Inorganic and Physical Chemistry, Alarich-Weiss-Straße 8, D-64287 Darmstadt, Germany. E-mail: gerd.buntkowsky@chemie.tu-darmstadt.de, gutmann@chemie.tu-darmstadt.de*

[b] *Free Universität of Berlin, Institute of Chemistry and Biochemistry, Takustraße 3, D-14195 Berlin, Germany*

[c] *LPCNO, INSA-CNRS-UPS, Institut National des Sciences Appliquées, Université de Toulouse, 135, Avenue de Rangueil, 31077 Toulouse, France. E-mail: romuald.poteau@univ-tlse3.fr*

† Electronic supplementary information (ESI) available. See DOI: 10.1039/d0cy02476g

nanoparticles on alumina or graphite have been intensively investigated for ammonia synthesis in the past few years (see *e.g.* ref. 17–23). Next to them, studies focused on ruthenium crystallites as catalysts as reviewed in ref. 24–26.

While many of these studies aimed at the preparation of novel nanoparticle catalyst systems for ammonia synthesis and for the formation of nitrogen containing organic compounds from ammonia, mechanistic studies are often limited to theoretical descriptions due to the high complexity of the surface chemistry on nanoparticles. In particular, the identification of surface species and reaction intermediates on these particles is a challenging task since standard techniques such as IR spectroscopy in many cases do not provide the necessary resolution. From the surface chemistry side, the role of NH_3 dissociation on ruthenium nanoparticles and its recovery after H_2 treatment have not been studied so far. Furthermore, to the best of our knowledge, the formation of urea upon reaction of ammonia with CO on ruthenium nanoparticles under mild conditions has not been monitored.

In the present work, we have studied the surface chemistry of ammonia on ruthenium nanoparticles (Ru NPs). Specifically, we have been interested in the adsorption of ammonia on these particles and its potential as a hydrogen vector. Furthermore, we investigate its reaction with co-adsorbed carbon monoxide. For this purpose, we have applied a combination of different solid-state NMR techniques including ^{15}N solid-state NMR. On the theoretical side, two main approaches are proposed: (i) mechanistic studies of the NH_3 and H_2 co-adsorption, followed by the study of possible reaction pathways of ammonia, accompanied or not by hydrogen desorption and (ii) DFT-based NMR studies that contribute to the safe assignment of NMR spectrum features. These two approaches require more thorough computational and theoretical studies in the near future, but they already provide some useful hints and trends with respect to the experimental data. As a model catalyst, we chose bis-diphenylphospinobutane (dppb) stabilized ruthenium nanoparticles containing surface hydrogen (Ru/H/dppb NPs) that can be produced *via* a synthetic protocol introduced by some of us.[27–29] For these particles, the synthesis protocol has been optimized and their texture structure has been well characterized using different analytical techniques such as transmission electron microscopy (TEM) or wide-angle X-ray scattering (WAXS).[30,31] The surface chemistry on ruthenium particles has been well studied in reactions with carbon monoxide and carbon dioxide by combination of different spectroscopic techniques including solid-state NMR as shown in several recent reviews.[32–37] Studies of nitrogen containing compounds on Ru NPs were performed for amino boranes as reviewed by Axet *et al.*[38] Very recently, the CO adsorption of Ru NPs stabilized by ^{15}N labeled nitrene ligands was investigated by Huang *et al.*[39] employing IR and ^{13}C CP MAS NMR. On the

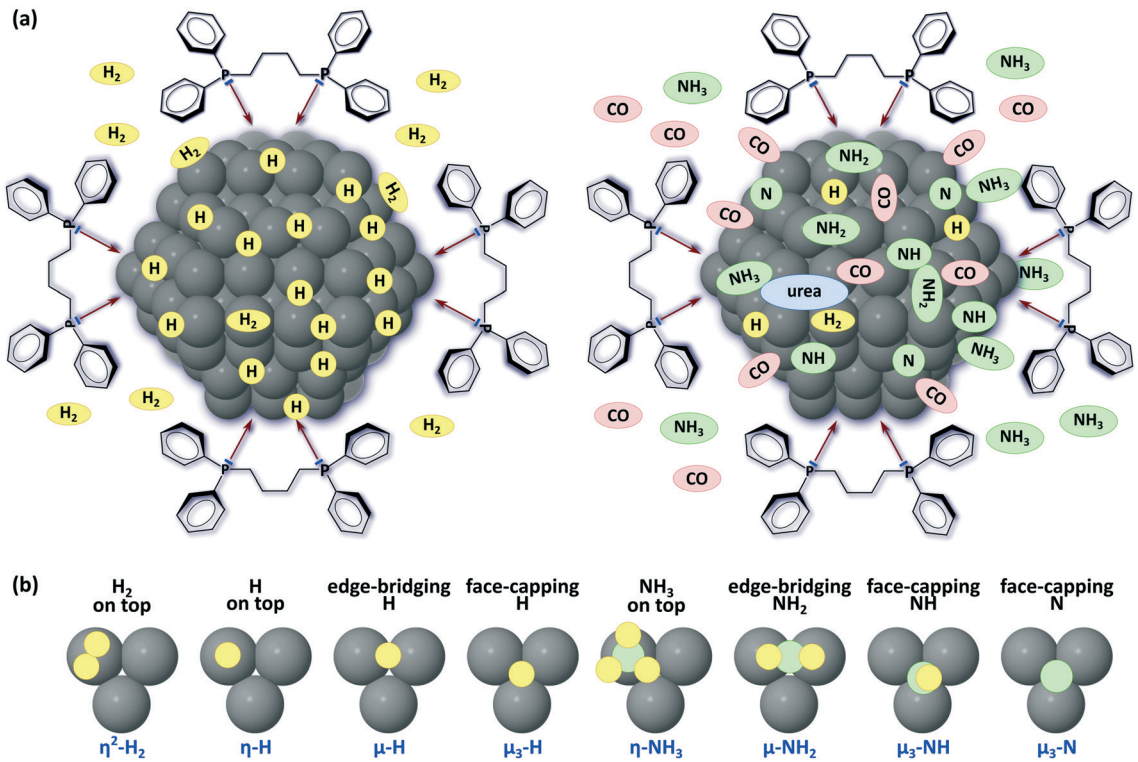

Fig. 1 (a) Schematic representation of presumed surface species on Ru/H/dppb NPs. Left side: Ru/H/dppb NPs covered with hydrogen species in different coordination modes. Right side: a model of Ru/H/dppb NPs showing feasible surface species after adsorption of NH_3 and co-adsorption of CO, respectively. (b) Coordination modes for H and NH_x (x = 0–3): (surface dihydrogen on top Ru(η^2-H_2), on top Ru(η-H), edge-bridging Ru(μ-H), face-capping Ru(μ_3-H), on top Ru(η-NH_3), edge-bridging Ru(μ-NH_2), face-capping Ru(μ_3-NH) and face-capping Ru(μ_3-N)).

edge of their work, a first ^{15}N CP MAS NMR spectrum obtained for ruthenium nanoparticles is shown. In addition, the reaction of ruthenium particles with molecular hydrogen has been the subject of intensive research in the past years. For example, different hydrogen binding sites such as on top Ru(η-H), edge-bridging Ru(μ-H) and face-capping Ru(μ_3-H) types, as well as on top surface dihydrogen Ru(η^2-H_2) (Fig. 1a, left side), have been identified experimentally by ^2H solid-state NMR studies on metallic nanoparticles[40] and molecular complexes or cluster compounds of ruthenium.[41,42] These experimental studies were underlined by results from quantum chemical calculations on ruthenium complexes and clusters.[43–45]

Furthermore, the mechanism behind the hydrogen adsorption on ruthenium nanoparticles has been studied in detail by a combination of gas-phase NMR and kinetic modelling. With this approach, an exchange mechanism has been confirmed where first, dihydrogen is adsorbed in an associative step followed by hydrogen transfer and an associated desorption step as illustrated on the right side in Fig. 3 in ref. 46.

To start, in this work, the following questions arose referring to mild conditions and gas pressures of a few bar: (i) How is NH_3 adsorbed on Ru/H/dppb NPs? (ii) Can surface nitrogen species be identified particularly by ^{15}N solid-state NMR techniques? To our knowledge, ammonia species on Ru NPs have not yet been studied by ^{15}N solid-state NMR. (iii) Is the formation of different nitrogen species controlled by the presence of hydrogen? (iv) Can adsorbed NH_3 react with other gases, in particular CO molecules under mild conditions after co-adsorption on Ru/H/dppb NPs without the presence of solvent, (Fig. 1a, right side) to form urea? The oxidative carbonylation of ammonia has been described before, using elevated temperatures and pressures, but sulfur[47,48] or selenium[49] had to be used as catalysts and reactants for uptaking the two hydrogen atoms released in the reaction. In the case of Ru NPs, this role could be taken by Ru surface atoms.

To answer these questions and to verify the proposed surface species, we first present the results of our ^{15}N solid-state NMR studies on the adsorption of NH_3 on Ru/H/dppbNPs followed by the results of the mechanistic studies on the NH_3 and H_2 co-adsorption on Ru_{55} model systems and quantum chemical calculations of ^{15}N chemical shifts on Ru_3 and Ru_6 clusters. Second, the results of ^{15}N and ^{13}C solid-state NMR studies when CO is co-adsorbed are shown. Based on these results, we will discuss the interaction and activation of NH_3 on the surface of Ru/H/dppb NPs. Finally, we will discuss the reaction of NH_3 and CO on the surface of Ru/H/dppb NPs and inspect the formation of urea on these particles.

Results

Adsorption of NH_3 on Ru/H/dppb NPs revealed by ^{15}N solid-state NMR techniques

As shown previously, after synthesis under 3 bar H_2 pressure, Ru NPs contain mobile surface hydrides of on top Ru(η-H), edge-bridging Ru(μ-H) and face-capping Ru(μ_3-H) types as well as surface dihydrogen on top Ru(η^2-H_2).[40,50] We placed these Ru/H/dppb NPs in an NMR rotor and exposed it to gaseous $^{15}NH_3$ at 2 bar and 60 °C for 60 h. After that, the resulting sample a was analyzed using solid-state ^{15}N CP MAS NMR. The resulting spectrum (Fig. 2, sample a) exhibits a narrow signal labelled A located at 24.5 ppm and two broad signals B and C centered at −12 and −42 ppm. Afterwards, sample a inside the rotor was exposed to a vacuum of 10^{-4} bar for 24 h resulting in a decrease of the narrow signal at 24.5 ppm (Fig. 2, sample b) while the intensity of the broad signals slightly increases. A similar effect was observed when some of the freshly prepared sample a was stored for 6 weeks at room temperature in a glove box under an argon atmosphere. The sharp signal at 24.5 ppm nearly completely disappeared (Fig. 2, sample c) and a broad dominating signal at about −35.5 ppm with a line width of about 1500 Hz (FWHM) remained.

To inspect the nature of the line broadening, T_2 measurements on ^{15}N were performed on sample c using the CP MAS echo sequence. Analysis of the obtained echo spectra for different echo spacings (see ESI† Fig. S2a) and fitting the data obtained from the signal areas with a mono exponential function (see ESI† Fig. S2b) led to a T_2 time constant of 6 ms,

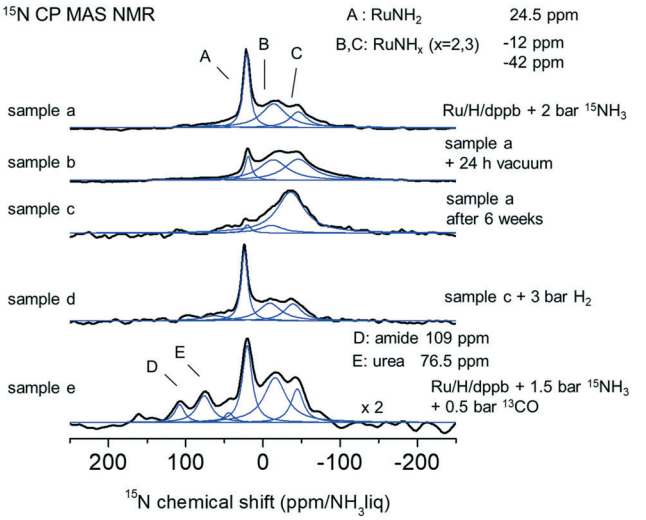

Fig. 2 ^{15}N CP MAS spectra of the Ru/H/dppb NP sample after adsorption of $^{15}NH_3$ and deconvolution of the signals. Sample a: the spectrum obtained after sample exposure to 2 bar $^{15}NH_3$ and heating at 60 °C for 60 h. Sample b: the spectrum obtained after exposure to a vacuum of 10^{-4} bar for 24 h. Sample c: the spectrum obtained after aging some of sample a at room temperature for 6 weeks. Sample d: the spectrum obtained after exposure to 3 bar H_2 at room temperature for 15 h. Sample e: the spectrum of the Ru/H/dppb sample after adsorption of $^{15}NH_3$ at 1.5 bar, heating at 50 °C for 3 days and subsequent co-adsorption of ^{13}CO at 0.5 bar and room temperature for 12 h. Note: the spectra were recorded at 5 kHz spinning. A line broadening of 200 kHz was applied. The spectra were normalized on the overall peak area. The spectrum of sample e is displayed with a vertical expansion factor of 2. The weak signals at 50 ppm to 75 ppm in the spectra were added in the deconvolution to represent the spectral shape in a better way. They cannot be assigned to specific surface sites.

corresponding to a natural line width of $\Delta\nu_{1/2}$ = 53 Hz. This value is much smaller than the signal line width indicating that the spectral shape is dominated by inhomogeneous line broadening arising from nuclei in magnetically different environments.

The spectral changes in the spectra of sample b and sample c compared to those of sample a lead to the assumption that dynamic processes on the nanoparticle surface occur which involve the activation or cleavage of the N–H bond. Similar observations are also found for the activation or cleavage of C–H and P–C bonds on Ru/dppb NPs.[51]

To verify this hypothesis, the aged particles (sample c) were exposed to 3 bar H_2 at room temperature for 15 h to inspect whether the aging is reversible. Interestingly, the ^{15}N CP MAS spectrum, which was acquired after hydrogen treatment, shows the recovery of the narrow signal at 24.5 ppm (Fig. 2, sample d).

To shed more light on the origin of the signals obtained in the ^{15}N CP MAS spectra, we applied spectral editing experiments on sample a to identify the different nitrogen containing species. We applied the non quaternary suppression (NQS)[52] technique by which dipolar couplings of immobile protons attached to ^{15}N can be detected. Fig. 3 shows the ^{15}N CPNQS spectrum of sample a obtained using an evolution time of 300 μs. For comparison, the ^{15}N CPNQS spectrum recorded using heteronuclear decoupling during the evolution is also depicted. It is obvious from this comparison that the sharp signal A at 24.5 ppm is not significantly affected by dipolar ^{1}H–^{15}N couplings while the intensities of the broad signals B and C decreased by more than 50%. This dephasing indicates that these signals arise from nitrogen species of type $RuNH_x$ affected by dipolar couplings. The finding that signal A is not dephased substantially does not indicate the absence of H bound to N,

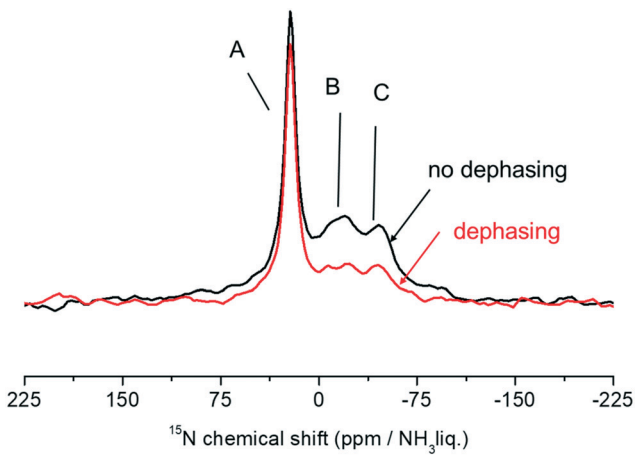

Fig. 3 Spectra of the freshly prepared Ru/H/dppb NP sample after adsorption of 2 bar $^{15}NH_3$ (sample a). Comparison of the ^{15}N CPNQS spectra recorded without (red spectrum, dephasing) and with (black spectrum, no dephasing) heteronuclear decoupling during the evolution.

but is consistent with $RuNH_x$ species which exhibit partial mobility which averages somewhat the dipolar ^{1}H–^{15}N couplings.

Finally, we analyzed the gas phase on the particles after the adsorption of NH_3 to identify the volatile species. For this, the gas phase on the freshly prepared Ru/H/dppb NPs after the adsorption of 2 bar NH_3 (sample a) was inspected under different conditions, namely (i) directly at room temperature, (ii) after applying a vacuum to sample a and treatment of argon, and (iii) after applying a vacuum to sample a and treatment of argon followed by heating at 120 °C. The GC-MS spectrum of the gas phase on each sample (exemplary shown for the sample prepared *via* approach iii, see ESI† Fig. S3) only shows the presence of NH_3 and Ar, which is a strong hint that volatile species such as hydrazine (NH_2–NH_2) are not present. To inspect the formation of species adsorbed on the surface of sample a at room temperature which can be easily removed, sample a was washed with 1 ml acetone and the solution was characterized *via* GC-MS. The detailed GC-MS analysis (see ESI† Fig. S4) clearly shows that the formation of hydrazine can be excluded; however, butane is visible which stems from the decomposition of parts of the dppb ligand system as studied in detail in a former work by some of us.[51]

Adsorption of NH_3 on Ru/H/dppb NPs revealed by quantum chemical calculations

Next to the experimental studies, quantum chemical calculations were performed to look at the thermodynamics of the NH_3 adsorption on Ru nanoparticles next to surface hydrogen/hydrides, and to predict ^{15}N chemical shifts to ease the interpretation of our experimental data.

(i) A thermodynamic study was first performed on a 1 nm Ru_{55} model, successfully used in previous joint theoretical/experimental studies.[53–56] All the structures, surface compositions and reaction energies considered in the present study are shown in Fig. 4. It is shown in Fig. 4 that the possible role of dppb has been neglected in these Ru_{55} models, which will be reintroduced only qualitatively in the discussion. Four hydride surface compositions were considered, from 0.0 $H/Ru_{surface}$ to 1.6 $H/Ru_{surface}$. In contrast, a unique and somewhat arbitrary ammonia composition was defined. An approach that would have been performed to calculate the Gibbs free energy of the adsorption of H_2 and NH_3 as a function of their chemical potentials was out of the scope of the present theoretical contribution. Yet, we shall see now that, without stabilizing ligands, this surface can host quite a large number of ammonia molecules. Twenty-two ammonia molecules stabilize the Ru_{55} nanocluster by 417 kcal mol^{-1}, *i.e.* 19.0 kcal mol^{-1} per NH_3, as shown in Fig. 4. Twenty-two hydrides stabilize Ru_{55} by 322 kcal mol^{-1} only (−14.6 kcal mol^{-1} per H), whereas the co-adsorption of 22 hydrides and 22 NH_3 is exothermic by −587 kcal mol^{-1} (for calculation details, see ESI† Table S2). Another energy clue consists in considering

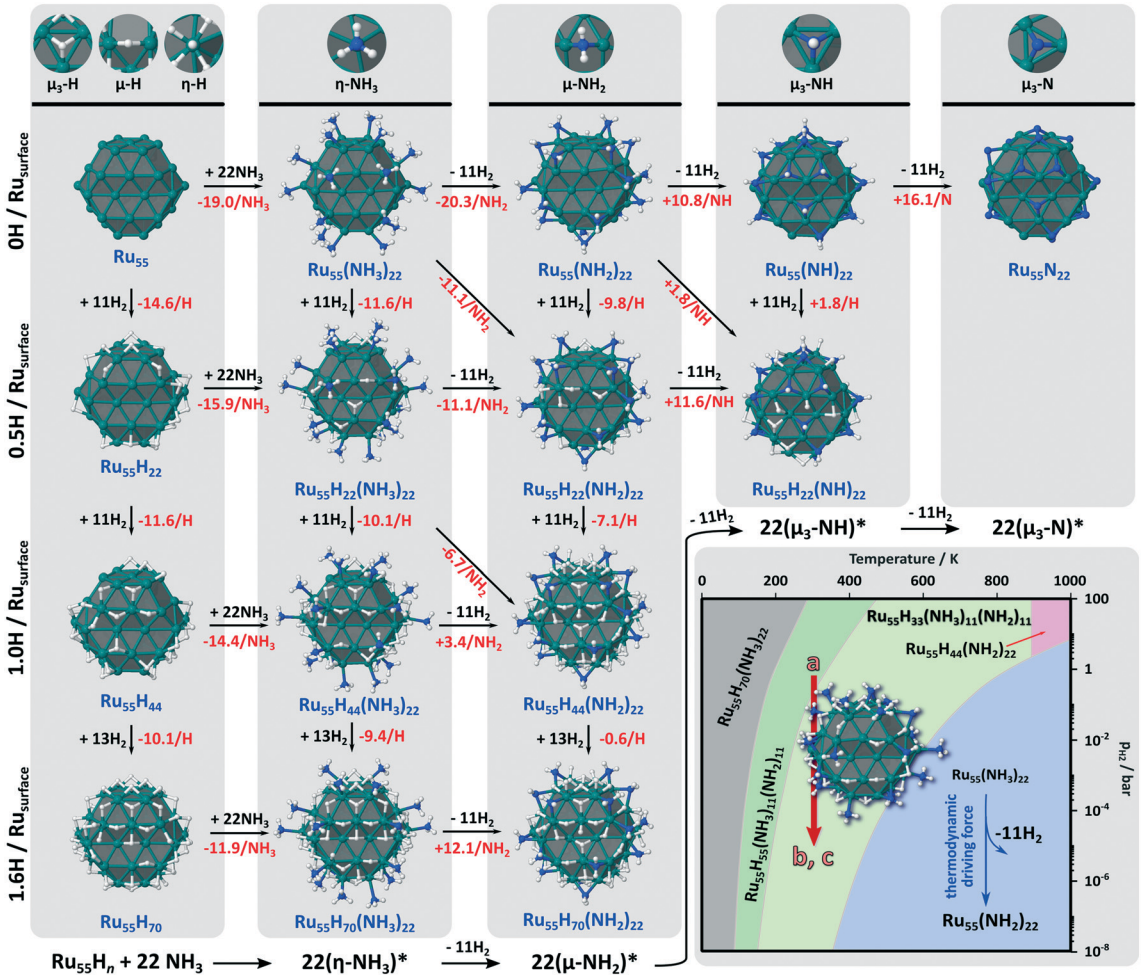

Fig. 4 Adsorption and decomposition energies of H_2 and ammonia at the surface of the 1 nm hcp Ru_{55} model. All energies (in red) are given in kcal mol^{-1}. Adsorption energies are calculated using the standard relationships given in the computational section. Horizontal reading: Reactions for the same H surface coverage from 0H/$Ru_{surface}$ (top) to 1.6H/$Ru_{surface}$ (bottom). The $Ru_{55}H_{70}$-derived models possess one non-dissociated H_2 molecule that may undergo a significant bond length variation as a function of local electronic effects. Global reactions from left to right are indicated in the footer of this figure. Diagonal reading: each NH_x decomposition reaction leaves both an NH_{x-1} and a hydride on the surface. The right inset contains a $\Delta G_{ads}(T, p_{H2})$ stability diagram calculated for a constant $(NH_x)_{22}$ composition. The red arrow represents the depletion of surface hydrides at *ca.* r.t. as a function of H_2 pressure, which could explain the variation of the ^{15}N CP MAS spectra observed between samples a, b and c (see text and computational details and additional explanations in the ESI.† All DFT energies are reported in Table S2†).

the adsorption energy of 22 NH_3 on a preformed $Ru_{55}H_{22}$ cluster. This process is exothermic by −15.9 kcal mol^{-1} per ammonia ligand (see Fig. 4). Given that hydrides are closer to the surface than adsorbed ammonia, (average Ru–N bond length: ~2.3 Å), the H/NH_3 competitive co-adsorption is ruled by electronic effects rather than by steric effects (a charge and electronic structure analysis of the selected compounds is given in the ESI† Table S1 and Fig. S6). And even on the hydride-rich $Ru_{55}H_{70}$ (= 1.6 H/$Ru_{surface}$), the adsorption of ammonia is still exothermic by −11.9 kcal mol^{-1} per NH_3. When compared to the average dissociative adsorption energy of 13 H_2 on $Ru_{55}H_{44}$ (−10.1 kcal mol^{-1} per H), it shows that even at such a high H coverage value, a high number of ammonia compounds can also adsorb on the surface and competitive adsorption/desorption processes of NH_3 and H_2 occur.

What is the chemical outcome of adsorbed ammonia molecules? After the activation of N–H on the surface, they can first decompose into NH_2 that will be coordinated to two Ru atoms. The barrier height is expected to be fairly low, as reported for example in ref. 57. The $Ru_{55}(NH_3)_{22}$ → $Ru_{55}(NH_2)_{22}$ reaction accompanied by the release of 11 H_2 molecules is exothermic by −20.3 kcal mol^{-1} per formed NH_2. The cost of a supplementary N–H bond breaking is however too high to favor the formation of μ_3-NH on the surface, even for undercoordinated surface Ru atoms ($Ru_{55}(NH_2)_{22}$ → $Ru_{55}(NH)_{22}$ + 11H_2: +10.8 kcal mol^{-1} per formed NH; even when H_2 is not released, the adsorption of H on the surface does not make the reaction exothermic, with the energy outcome being +1.8 kcal mol^{-1} per formed NH). The final formation of μ_3-N seems totally impossible without an external assistance such as a thermodynamic driving force.

As can be seen in Fig. 4, it is even worse when starting from $Ru_{55}H_{22}$. The conversion from $Ru_{55}(NH_2)_{22}$ to $Ru_{55}H_{22}(NH)_{22}$ on such a hydrogen-poor surface suggests a possible equilibrium between HN* and H_2N* (ΔE = +1.8 kcal mol^{-1} per NH). But under H_2 pressure, the thermodynamic driving force will lead to H_2N* ($Ru_{55}H_{22}(NH)_{22}$ + 11 H_2 → $Ru_{55}H_{22}(NH_2)_{22}$: ΔE = −11.6 kcal mol^{-1} per formed NH_2). In conclusion, the formation of HN* and N* is unlikely. Let us now obey the exothermic processes shown in Fig. 4, starting from $Ru_{55}H_{22}(NH_2)_{22}$. They suggest that with 22 amine-derived compounds, the optimal surface coverage can reach 1.6 H/$Ru_{surface}$, with NH_3 only (*i.e.* $Ru_{55}H_{70}(NH_3)_{22}$). But since DFT calculations are implicitly done for T = 0 and no external pressure or concentration of adsorbates, this situation does not account for real experimental conditions. Such study is well beyond the scope of the present work (it would involve considering several ammonia compositions, using the so-called *ab initio* thermodynamics). But such a method can bring interesting trends, even if achieved on a subset of structures. This is what has been done to establish the $\Delta G_{ads}(T, p_{H2})$ stability diagram shown in the inset of Fig. 4 (see also the computational details in the ESI†). All the $Ru_{55}H_n(NH_3)_{22}$ structures have been considered there, complete with $Ru_{55}H_{33}(NH_3)_{11}(NH_2)_{11}$ and $Ru_{55}H_{55}(NH_3)_{11}(NH_2)_{11}$. The former (green domain) is the most stable at *ca.* r.t. and exposure to 1 bar H_2, whereas the latter (yellow domain) appears to be the most stable at the same temperature and at a lower hydrogen pressure. At a relatively high temperature, the NPs not subjected to a constant pressure of hydrogen yield ammonia only-stabilized nanoclusters ($Ru_{55}(NH_3)_{22}$). Given the aforementioned −20.3 kcal mol^{-1} that accompanies the decomposition of ammonia into H_2N*, the resulting NPs under a very low hydrogen pressure and high temperature will most probably be stabilized by NH_2, strongly adsorbed on various coordination sites (blue domain in Fig. 4).

The effect of temperature, ammonia or hydrogen pressure and surface stabilizers such as dppb will of course change these numbers, but the final conclusion is expected to hold, *i.e.* probable coexistence of hydrides, NH_3 and NH_2 on the surface and depletion of surface hydrides after exposure to vacuum. The same phenomenon is expected to occur after aging, given the weaker adsorption energies of hydrides with respect to NH_3 or NH_2. A confirmation of these qualitative trends is needed. It will be done in the discussion part by confronting the following DFT-based NMR chemical shifts and experimental NMR observations.

(ii) Given that NMR chemical shifts are mainly sensitive to local environments, we have considered small clusters with a variable number of surface species, to mimic the undercoordination at the surface of RuNPs. This strategy was successfully applied to ^{1}H NMR, ^{13}C NMR (see computational details) and ^{15}N NMR.[58] Forty-six clusters were computed in the present work, with adsorbed ammonia, H_2N*, HN*, N*, hydrazine, and urea with or without ammonia in the second coordination sphere making hydrogen bonds with adsorbed species. Detailed results are presented in Fig. S7.† The rather large number of compounds allows us to identify the ^{15}N NMR domains for all these species. These domains are shown in Fig. 5. Ammonia is characterized by a negative or null chemical shift, whatever its coordination; regular unshielding is observed upon the successive N–H activations; H_2N* is usually downfield shifted with respect to H_3N*, with 60 ppm > δ > −10 ppm (red domain in Fig. 5), with the noticeable exception of clusters undercoordinated and stabilized only by NH_3 or NH_2, *i.e.* without surface hydrides or CO (green domain in Fig. 5); HN* and N* resonate at low fields (δ > 190 ppm, with the exception of NH adsorbed on strongly distorted sites, green domain in Fig. 5); hydrazine and urea should be observed between ~0 and 70 ppm, *i.e.* it will not be easy to differentiate their signals from H_2N* in case of co-adsorption.

Co-adsorption of NH_3 and CO on Ru/H/dppb NPs revealed by ^{15}N and ^{13}C CP MAS NMR

In the next stage of this study, we inspected the reactivity of surface ammonia species towards carbon monoxide, which exhibits a C1 unit to form organic compounds. For this purpose, freshly prepared Ru/H/dppb NPs were firstly treated with 1.5 bar $^{15}NH_3$ and heated for 3 days at 50 °C. Then, they were treated with 0.5 bar ^{13}CO at room temperature for 12 h leading to sample e studied by solid-state NMR techniques.

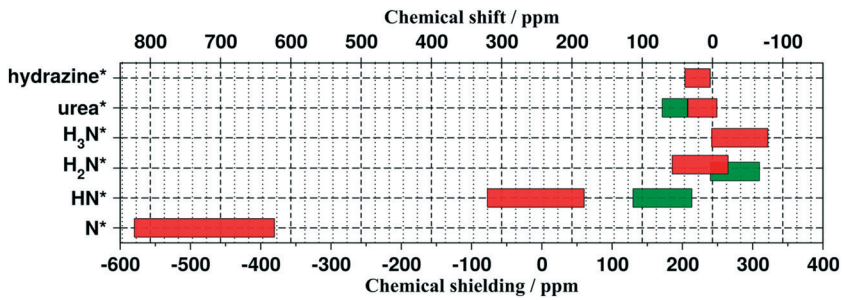

Fig. 5 ^{15}N NMR domains, on the basis of PBE0-DFT calculations on 46 Ru_6 clusters and 3 Ru_3 clusters. Urea: green and red for σ- and π-coordinated urea, respectively (see ESI† Fig. S8 for structures). NH_2: green for some pure $Ru_6(NH_2)_x$ clusters and red for other cases (see text). NH: green for small fully saturated Ru_3 clusters or strongly distorted [Ru_6] clusters. See Fig. S7† for more details and 3D representations of some clusters.

Comparison of the ^{15}N CP MAS spectra of the freshly prepared Ru/H/dppb NPs after the adsorption of $^{15}NH_3$ (Fig. 2, sample a) and after the co-adsorption of ^{13}CO (Fig. 2, sample e) shows that two new signals (at 109 and 76.5 ppm) have appeared after the co-adsorption of ^{13}CO. The signal at 76.5 ppm is in the typical range for nitrogens in urea as supported by the reference spectrum of ^{15}N labelled urea (ESI† Fig. S5a). The signal at 109 ppm is characteristic of nitrogens in amide groups whose origin will be discussed in the Discussion section.

^{13}C CP MAS spectra were recorded to shed more light on carbon containing species. Comparison of the ^{13}C CP MAS spectrum of the freshly prepared Ru/H/dppb NPs (Fig. 6, sample f) with the spectrum of the freshly prepared Ru/H/dppb NPs after the adsorption of $^{15}NH_3$ at 1.5 bar and heating at 50 °C for 3 days (Fig. 6, sample g) shows that they exhibit strong signals at similar positions in the aliphatic region (10–50 ppm) and some weak signals in the aromatic region (120–140 ppm). This implies that the adsorption of NH_3 has no significant influence on the chemical environment of the present carbon species, which mainly refer to the dppb ligand system, remaining solvent molecules and probably hydrogenation or decomposition products.[30,51]

The situation changes when ^{13}CO is co-adsorbed. As shown by the deconvolution of the ^{13}C CP MAS spectrum of sample e (Fig. 6, right panel), three additional signals with significant intensities appear at 220, 195.5 and 161.5 ppm, as well as a tiny signal at 128.5 ppm. The broad signal at 220 ppm contains no visible spinning sidebands and is typical for CO molecules in a bridged coordination as shown by some of us in previous studies.[30,59] For the central signal at 195.5 ppm, spinning sidebands are visible marked with asterisks. This observation clearly indicates that the carbon species assigned to this signal exhibit a significant chemical shift anisotropy. According to our previous work on CO adsorption on Ru/dppb nanoparticles, this signal can be attributed to terminally bound CO in a rigid mode.[30] A more detailed analysis of the chemical shift anisotropy tensor, as done by Mafra and co-workers[60] for ^{13}C spectra of amine functionalized porous silica after adsorption of ^{13}CO, is not feasible in a serious way for our spectrum due to the low S/N ratio. Finally, the signal at 161.5 ppm containing no visible spinning sidebands is in the typical range of carbonyl carbons in urea and derived compounds as shown in ref. 61 and 62 and underlined by the ^{13}C CP MAS NMR reference spectrum of ^{15}N labelled urea (ESI† Fig. S5b).

Discussion

Adsorption and reactions of NH_3 on Ru/H/dppb NPs

The ^{15}N CP MAS spectrum obtained for the Ru/H/dppb NPs after the adsorption of $^{15}NH_3$ (Fig. 2, sample a) clearly shows that NH_3 from the gas phase is bound on the surface of the Ru nanoparticles and becomes part of the solid, *i.e.* it is chemisorbed. The question arises which surface species are formed and whether they can be identified by solid-state NMR. For that purpose, we discuss the following surface–gas equilibria.

$$RuH_{n-2} + H_{2gas} \rightleftarrows RuH_n \quad (1)$$

$$Ru_mH_n + NH_{3gas} \rightleftarrows Ru_mH_{n-2}(NH_3) + H_{2gas} \quad (2)$$

$$Ru_mH_{n-2}(NH_3) \rightleftarrows Ru_mH_{n-1}(NH_2) \rightleftarrows Ru_mH_{n-2}(NH_2) + {}^1/_2H_{2gas} \quad (3)$$

$$Ru_mH_{n-2}(NH_2) \rightleftarrows Ru_mH_{n-1}(NH) \rightleftarrows Ru_mH_{n-2}(NH) + {}^1/_2H_{2gas} \quad (4)$$

$$Ru_mH_{n-2}(NH) \rightleftarrows Ru_mH_{n-1}N \rightleftarrows Ru_mH_{n-2}N + {}^1/_2H_{2gas} \quad (5)$$

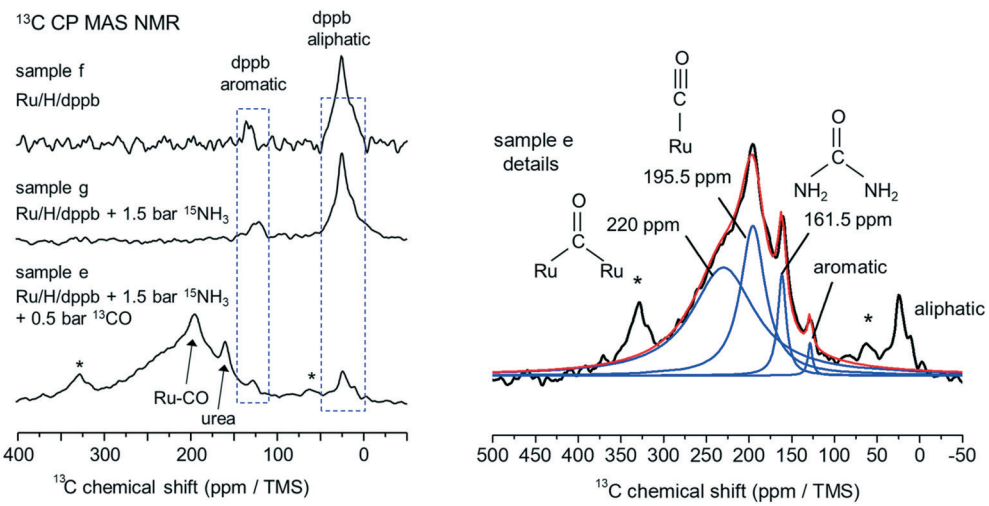

Fig. 6 Left panel: ^{13}C CP MAS spectra of the freshly prepared Ru/H/dppb NPs (sample f), freshly prepared Ru/H/dppb NPs after the adsorption of $^{15}NH_3$ at 1.5 bar and heated at 50 °C for 3 days (sample g) and freshly prepared Ru/H/dppb NPs after the adsorption of $^{15}NH_3$ at 1.5 bar, heated at 50 °C for 3 days and treatment with ^{13}CO at 0.5 bar at room temperature for 12 h (sample e). Right panel: Deconvolution of the broad signal obtained for sample e. Note: the spectra are normalized to their maximum signal intensity. Spinning sidebands are marked by asterisks.

As illustrated in Fig. 1a (left side), after the synthesis, the Ru NPs are fully covered with surface hydrogen in equilibrium with gaseous H_2 as stated in eqn (1). The different coordination modes are illustrated in Fig. 1b. Eqn (1) was corroborated by the former finding that the treatment of RuNPs with D_2 (ref. 40 and 46) leads to a release of HD and H_2 into the gas phase. The ^{15}N CP MAS NMR experimental results depicted in Fig. 2 indicate that when the NH_3 gas is exposed to Ru NPs, it is strongly bound to the surface. It follows that H_2 must be released according to eqn (2), where the first reaction step corresponds to the formation of $RuNH_3$ species.

However, the ^{15}N CP MAS NMR experiments are not compatible with only a single ammonia surface species. Therefore, we considered the reactions depicted in eqn (3) to (5) where hydrogen atoms are successively dissociated from nitrogen to fill up the surface hydrogen reservoir and eventually produce gaseous dihydrogen. This means that under the conditions where the reaction was performed in this study, *i.e.* adsorption at room temperature followed by heating at 60 °C for 60 h and a gas pressure of a few bar, the amount of hydrogen on the surface and in the gas phase may influence which nitrogen surface species are formed. However, to determine which reaction occurs in the present case and which ammonia surface species, it was necessary to assign the observed ^{15}N chemical shifts as described in the following.

^{15}N chemical shift assignments of surface ammonia species on Ru NPs assisted by quantum-chemical calculations

For that purpose, a number of DFT calculations were performed. ^{15}N chemical calculations were performed on Ru_6 model clusters and energy and structure calculations on Ru_{55} model clusters. The results of these DFT calculations are summarized in Fig. 4 and 5. The formation of RuNH and RuN species (eqn (4) and (5)) was shown to be thermodynamically unstable and hence unlikely under the conditions used experimentally. This was corroborated by the finding that the ^{15}N chemical shifts (reference liquid external NH_3) of RuN should be found in the 800–600 ppm range and of RuNH in the 300–200 ppm range which are far away from signals A, B and C in Fig. 2. Therefore, $RuNH_3$ and $RuNH_2$ are the only candidates for these signals. As depicted in Fig. 5, the normal range for $RuNH_2$ was found to be between 60 and −20 ppm, in particular in the neighbourhood of Ru saturated with hydrogen. The value of 24.5 ppm of signal A corresponds to this region. In contrast, high-field shifts in the range of 0 to −60 ppm are calculated for $RuNH_2$ on Ru surfaces depleted with surface hydrogen. This range is similar to the one found for $RuNH_3$. Therefore, it is difficult to distinguish the latter two species. In other words, signals B and C can both correspond to $RuNH_2$ in hydrogen poor Ru surfaces and to $RuNH_3$. Thus, it is understandable that signal A is reduced by removing hydrogen from the gas phase, and that the quite broad signals B and C increased in intensity, without a change in the fractions of $RuNH_2$ and $RuNH_3$. This is further corroborated by the inset of Fig. 4 which depicts a partial phase diagram. It tells us that when reducing the H_2 gas pressure from a few bar to very low pressures, the ratio of $RuNH_2$ to $RuNH_3$ should remain constant.

Finally, we note that signal A is relatively sharp as compared to signals B and C. This may arise from partial mobility of $RuNH_2$ on a hydrogen-rich surface. This is also indicated in the NQS spectrum (Fig. 3) in which only a slight dephasing is obtained for signal A, which is related to an averaging of the heteronuclear dipolar interaction. In contrast, an inhomogeneous distribution of surface sites and/or coordination modes (Fig. 1b and 4) could be expected for the hydrogen-poor surfaces. However, the data do not allow us to distinguish such sites at the present time.

Co-adsorption of NH_3 and CO on Ru/H/dppb NPs

In the previous section, the chemisorption of NH_3 on Ru/H/dppb NPs and its reactions were discussed in detail. Now, the question arose what happens when a second molecule, namely CO is co-adsorbed. In this case, the surface reactions of NH_3 described above take place, which is visible by the appearance of signals A, B and C in the ^{15}N CP MAS spectrum of sample e (Fig. 2). In parallel, the typical surface chemistry of CO[30] occurs as visible in the spectral pattern of the ^{13}C CP MAS spectrum of sample e (Fig. 6). Next, in these surface reactions an additional major reaction occurs, *i.e.* the formation of urea, which is supported by the occurrence of signal E at 76.5 ppm in the ^{15}N CP MAS spectrum (Fig. 2) and the signal at 161.5 ppm in the ^{13}C CP MAS spectrum (Fig. 6) of sample e. The ^{15}N CP MAS spectrum also contains an additional signal D at 109 ppm whose origin is discussed below.

The question then arises how urea is formed on the surface of the Ru/H/dppp NPs and how it is interacting with the surface. We assume a consecutive addition of amino groups to bound CO according to eqn (6).

$$\begin{aligned} &RuNH_2 + RuCO \rightleftarrows Ru + RuCONH_2 \\ &RuNH_2 + RuCONH_2 \rightleftarrows Ru + RuNH_2CONH_2 \end{aligned} \quad (6)$$

Fig. 7 depicts the possible structures of the species involved. In the first step, CO has to be adsorbed on the particles' surface and next to it, two $RuNH_2$ sites have to be present. While the formation of the RuCO site may occur directly when CO is adsorbed on the Ru/H/dppb NPs, the formation of $RuNH_2$ proceeds *via* the equilibrium reactions described in the previous section. Then, a $RuNH_2$ group may bind to an adjacent RuCO group forming an amide like $RuCONH_2$ reaction intermediate, in which a coordination to Ru *via* the carbon is assumed. Such a reaction intermediate might be a candidate which could explain signal D at 109 ppm in the ^{15}N CP MAS spectrum of sample e which is typical for nitrogen in amide bonds. A clear assignment of this signal would however need further corroboration which is beyond the scope of the present work.

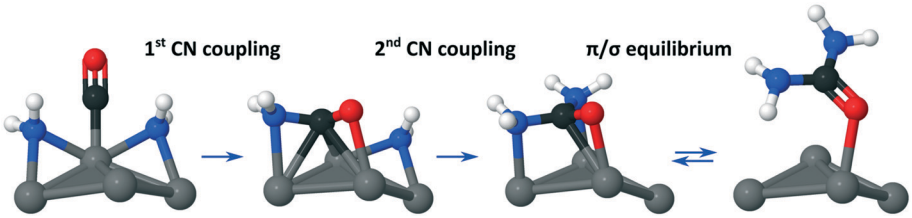

Fig. 7 Possible mechanism of the formation of urea from $RuNH_2$ and CO bound to Ru nanoparticles. The coordination modes were inferred after DFT calculations on a Ru_{13} model cluster.

In a subsequent reaction step, a second $RuNH_2$ species reacts with $RuCONH_2$ and forms surface-bound urea. A π-coordination between Ru and the CO group of urea is slightly more favorable than the σ-coordination to Ru of the oxygen of urea as calculations for a simple $Ru_{13}H_{17}$ model cluster show (−21.5 kcal mol^{-1} *vs.* −16.6 kcal mol^{-1}, see Fig. S7 and S8†). The calculations (Fig. 5 and ESI† Fig. S7) indicate that there is no large difference between the ^{15}N chemical shifts of the two coordination modes. Moreover, the ^{15}N and ^{13}C CP MAS signal positions of urea are very similar to those of neat urea (see ESI† Fig. S3). Therefore, it is difficult at present to distinguish both coordination modes. The absence of spinning sidebands of signal E in the ^{13}C CP MAS spectrum of sample e (Fig. 6) indicates that the urea is not very rigidly bound to the Ru/H/dppb NPs.

Experimental section

Materials

The precursor Ru(COD)(COT) was purchased from Umicore. The 1,4-bis(diphenylphosphino)butane (dppb) ligand was bought from Sigma-Aldrich. These reagents were used without further purification. Pentane and THF were purchased from Carl Roth in synthesis grade quality. Pentane was distilled over sodium and THF over CaH_2 to remove residual water. The solvents were degassed by three freeze pump cycles to remove dissolved oxygen.

Synthesis of Ru/H/dppb NPs

Ru/H/dppb NPs were prepared by following the procedure described by Novio *et al.*[30] using a 250 ml Fisher–Porter bottle which could be attached to a vacuum of <1 mbar or argon and hydrogen gas supplies. Typically, 200 mg (0.63 mmol, 1 eq.) Ru(COD)(COT) were placed in a Fisher–Porter bottle and dissolved in 120 mL dried and degassed THF forming a bright yellow solution. The solution was cooled down with a mixture of ethanol cooled with liquid N_2 (−116 °C). Under fast stirring, a solution containing 27 mg (63 μmol, 0.1 eq.) 1,4-bis(diphenylphosphino)butane (dppb) in 80 mL dried and degassed THF was slowly added to the cooled solution. The reaction mixture was then left to reach room temperature. After applying a partial vacuum, the Fisher–Porter bottle was pressurized with 3 bar of hydrogen gas. After stirring the solution under H_2 atmosphere for 30 min, the bright yellow solution turned black. The mixture was then stirred at room temperature for 18 h under an H_2 atmosphere. The volume of the reaction mixture was reduced to approximately 10 mL by vacuum distillation. Ruthenium nanoparticles were then precipitated by adding 80 mL of cold, dried and degassed pentane. This mixture was stirred for 10 min and filtered under an argon atmosphere. The particles were washed with 35 mL pentane two times and dried under vacuum to obtain the Ru/H/dppb NPs as a black powder.

Adsorption of $^{15}NH_3$ on the Ru/H/dppb NPs

The adsorption of $^{15}NH_3$ was performed in a 5 ml Fisher-Porter bottle by inserting an opened NMR rotor filled with the freshly prepared Ru/H/dppb NPs into the bottle. A vacuum was applied to the Fisher–Porter bottle for at least 30 min. Then, the bottle was pressurized with 2 bar $^{15}NH_3$ and heated with an oil bath to 60 °C for 60 h. Before using the particles in NMR experiments, a vacuum was applied for approximately 30 min, to remove gaseous ammonia (sample a).

Co-adsorption of ^{13}CO next to $^{15}NH_3$ on the Ru/H/dppb NPs

Co-adsorption of ^{13}CO was performed on a Ru/H/dppb NP sample with adsorbed $^{15}NH_3$. The adsorption of $^{15}NH_3$ was performed, similar to sample a by treating a freshly prepared Ru/H/dppb NP sample with 1.5 bar $^{15}NH_3$ and heating it for 3 days at 50 °C (sample g). Under an argon atmosphere, the sample was packed into a 4 mm ZrO_2 rotor and placed into a 5 mL Fisher–Porter bottle. After applying a vacuum, the Fisher–Porter bottle was treated with 0.5 bar of ^{13}CO gas and stored for 12 h at room temperature (sample e). Excess ^{13}CO was then removed under reduced pressure and the rotor was closed under an argon atmosphere with a driving cap before placing into the spectrometer.

Solid-state NMR

All solid-state NMR experiments were carried out at 7 T on a Bruker Avance III spectrometer corresponding to frequencies of 300.00 MHz for ^1H, 75.46 MHz for ^{13}C and 30.40 MHz for ^{15}N. This spectrometer is equipped with a 4 mm H/X double resonance probe. ^{15}N CP MAS experiments were performed at a spinning rate of 5 kHz (samples a–d) and 6 kHz (sample e) with a contact time of 4 ms employing a linear 50–100 ramp. 4096 to 15 360 scans were applied with a repetition delay of 2 s corresponding to measurement times between 3 and 8.5 h

for each spectrum. Acquisition times were set between 5 and 30 ms.

^{13}C CP MAS experiments were performed at a spinning rate of 6 kHz (sample f and g) and 10 kHz (sample e) with a contact time of 3 ms employing a linear 50–100 ramp. 3500 to 15 360 scans were applied with a repetition delay of 4 s corresponding to measurement times between 4 and 17 h for each spectrum. Acquisition times were set to 10 ms. The ^{1}H excitation pulse length for CP experiments was set to 4 μs. ^{1}H decoupling was performed using the two-pulse phase modulation (TPPM) sequence.[63]

To inspect the nature of line broadening of the signals in the upfield region of the ^{15}N CP MAS spectra, an exemplary T_2 measurement was performed on sample c since for this sample, the broad signals are dominating which eases the data analysis. For this measurement, the CP sequence was modified by adding a π pulse on the ^{15}N channel to generate echoes. The π pulse length on the ^{15}N channel was set to 10 μs. Spectra were recorded with different echo-spacings of 0.9, 1.5, 2, 4, 8 and 10 ms, respectively. Each single spectrum was recorded with 12 288 scans and a repetition delay of 1 s corresponding to an overall measurement time of *ca.* 20 h. For data analysis, the broad signals were reproduced with a Voigt line centered at −28 ppm from which the peak area was determined. Fitting was performed with a monoexponential function.

^{15}N and ^{13}C chemical shift referencing

The ^{15}N chemical shifts were referenced to the value of liquid $^{15}NH_3$ at 25 °C. The latter resonates at −381.7 ppm with respect to nitromethane[64,65] or at 40 ppm upfield from solid $^{15}NH_4Cl$ (ref. 66) which was used as the external reference in the experiments. The ^{13}C chemical shifts were given with respect to TMS employing the C═O signal of glycine (176.5 ppm) as an external reference.

Spectral editing experiments

To modulate the signal intensities in the ^{15}N spectrum under the influence of heteronuclear dipolar couplings, the non quaternary suppression (NQS) experiment[52] was performed on the sample of freshly adsorbed ammonia on Ru/dppb NPs (sample a). The experiment was set employing the Bruker pulse sequence cpnqs implemented in Topspin 3.2. Typically, a 4 μs excitation pulse was applied on ^{1}H and a π pulse of 8.5 μs on ^{15}N. The recycle delay was set to 2 s and an evolution time of d_3 = 300 μs was utilized. For comparison, the non quaternary suppression (NQS) experiment was performed with heteronuclear decoupling during the evolution. The pulse sequences employed for the experiments are given in the ESI† Fig. S1.

Computational details

They are reported in the ESI.†

Conclusions

In this study, we have used solid state ^{15}N and ^{13}C CP MAS NMR spectroscopy and DFT calculations to study the adsorption of $^{15}NH_3$ and the co-adsorption of $^{15}NH_3$ and CO on hydrogen containing Ru nanoparticles stabilized with dppb. From the discussion of the experimental and theoretical results, the following conclusions can be derived:

(i) When the Ru/H/dppb NPs, which are saturated with hydrogen, are exposed to gaseous $^{15}NH_3$, the latter is adsorbed on the surface and is chemisorbed, *i.e.* bound to Ru.

(ii) Three ^{15}N signals A, B and C have been observed for the chemisorbed ammonia. Assisted by the DFT calculations on Ru_6 clusters, the formation of RuN and RuNH species could be excluded. Evidence was obtained for the presence of comparable amounts of $RuNH_3$ and $RuNH_2$. The latter is formed by the dissociation of the former after chemisorption and H-transfer to surface Ru atoms. The ^{15}N chemical shifts of $RuNH_2$ are different for hydrogen-rich and hydrogen-poor surface environments which lead to spectral changes when hydrogen is removed from the Ru surface.

(iii) Co-adsorption of NH_3 and CO produces surface bound urea under mild conditions as observed by ^{15}N and ^{13}C CP MAS NMR. The urea molecules formed are most probably σ-coordinated to the surface *via* Ru–O bonds, but the π-coordination of the CO group of urea to Ru cannot be completely excluded.

(iv) There are a number of remaining open questions, both experimental and theoretical ones. In future experiments, one could try to verify and explore in more detail the current partial phase diagram in Fig. 4. For example, at low temperatures and high hydrogen pressures, one could expect that all $RuNH_2$ species are converted into $RuNH_3$ which should lead to interesting spectral changes after heating and exposure to vacuum. Thus, one may better distinguish $RuNH_2$ and $RuNH_3$ species *via* ^{15}N solid state NMR. Also, ^{1}H NMR experiments would be helpful to detect ammonia and hydrogen in the gas phase. DFT calculations on a number of different model systems even including the stabilizing ligands could include pressure variations of ammonia in the gas phase as a variable. The role of the surface composition of the N–H activation barrier and the investigation of the mechanism of the formation of urea or other derivatives would also bring further insights.

(v) We hope that the present study opens up a new fruitful field of research on ammonia on metal nanoparticles by solid state NMR and DFT calculations.

Conflicts of interest

There are no conflicts to declare.

Acknowledgements

This work was supported by the DFG under contract BU-911-26-1. IdR and RP thank the CALMIP HPC for a generous

allocation of computational resources (Olympe machine, grant P0611). GM thanks the European Union's Horizon 2020 research and innovation program under the FET-OPEN Grant Agreement No. 862179 for funding.

References

1 W. Ostwald, Improvements in the Manufacture of Nitric Acid and Nitrogen Oxides, *GB Pat.*, 190200698A, 1902.
2 C. Bosch and W. Meiser, Process of Manufacturing Urea, *US Pat.*, 1429483A, 1922.
3 M. Appl, in *Ullmann's Encyclopedia of Industrial Chemistry*, 2006, DOI: 10.1002/14356007.a02_143.pub2.
4 S. L. Miller and H. C. Urey, *Science*, 1959, **130**, 245–251.
5 S. P. Thoms, *Ursprung des Lebens*, Fischer Kompakt, Frankfurt, 2005.
6 P. Ehrenfreund, W. Irvine, L. Becker, J. Blank, J. R. Brucato, L. Colangeli, S. Derenne, D. Despois, A. Dutrey, H. Fraaije, A. Lazcano, T. Owen, F. Robert and ISSI-Team, *Rep. Prog. Phys.*, 2002, **65**, 1427–1487.
7 J. I. van der Vlugt, *Chem. Soc. Rev.*, 2010, **39**, 2302–2322.
8 F. Haber and R. L. Rossignol, Production of Ammonia, *US Pat.*, 971501A, 1910.
9 C. Bosch, The development of the chemical high pressure method during the establishment of the new ammonia industry, *Report Nobel Lecture*, 1932.
10 G. Ertl, D. Prigge, R. Schloegl and M. Weiss, *J. Catal.*, 1983, **79**, 359–377.
11 R. Schlögl, *Angew. Chem.*, 2003, **115**, 2050–2055.
12 K. Honkala, A. Hellman, I. N. Remediakis, A. Logadottir, A. Carlsson, S. Dahl, C. H. Christensen and J. K. Norskov, *Science*, 2005, **307**, 555–558.
13 G. Ertl, *Angew. Chem., Int. Ed.*, 2008, **47**, 3524–3535.
14 J. Qian, Q. An, A. Fortunelli, R. J. Nielsen and W. A. Goddard, *J. Am. Chem. Soc.*, 2018, **140**, 6288–6297.
15 F. Rosowski, A. Hornung, O. Hinrichsen, D. Herein, M. Muhler and G. Ertl, *Appl. Catal., A*, 1997, **151**, 443–460.
16 O. Hinrichsen, F. Rosowski, A. Hornung, M. Muhler and G. Ertl, *J. Catal.*, 1997, **165**, 33–44.
17 A. Miyazaki, L. Balint, K. Aika and Y. Nakano, *J. Catal.*, 2001, **204**, 364–371.
18 S. J. Guo, X. L. Pan, H. L. Gao, Z. Q. Yang, J. J. Zhao and X. H. Bao, *Chem. – Eur. J.*, 2010, **16**, 5379–5384.
19 Z. Song, T. H. Cai, J. C. Hanson, J. A. Rodriguez and J. Hrbek, *J. Am. Chem. Soc.*, 2004, **126**, 8576–8584.
20 C. Fernandez, C. Sassoye, D. P. Debecker, C. Sanchez and P. Ruiz, *Appl. Catal., A*, 2014, **474**, 194–202.
21 C. Fernandez, N. Bion, E. M. Gaigneaux, D. Duprez and P. Ruiz, *J. Catal.*, 2016, **344**, 16–28.
22 J. M. Zhao, J. D. Zhou, M. W. Yuan and Z. X. You, *Catal. Lett.*, 2017, **147**, 1363–1370.
23 C. Leterme, C. Fernandez, P. Eloy, E. M. Gaigneaux and P. Ruiz, *Catal. Today*, 2017, **286**, 85–100.
24 N. Saadatjou, A. Jafari and S. Sahebdelfar, *Chem. Eng. Commun.*, 2015, **202**, 420–448.
25 G. Z. Chen, J. M. Zhang, A. Gupta, F. Rosei and D. L. Ma, *New J. Chem.*, 2014, **38**, 1827–1833.
26 A. Ishikawa, T. Doi and H. Nakai, *J. Catal.*, 2018, **357**, 213–222.
27 C. Amiens, B. Chaudret, D. Ciuculescu-Pradines, V. Colliere, K. Fajerwerg, P. Fau, M. Kahn, A. Maisonnat, K. Soulantica and K. Philippot, *New J. Chem.*, 2013, **37**, 3374–3401.
28 B. Chaudret and K. Philippot, *Oil Gas Sci. Technol.*, 2007, **62**, 799–817.
29 C. Pan, K. Pelzer, K. Philippot, B. Chaudret, F. Dassenoy, P. Lecante and M. J. Casanove, *J. Am. Chem. Soc.*, 2001, **123**, 7584–7593.
30 F. Novio, K. Philippot and B. Chaudret, *Catal. Lett.*, 2010, **140**, 1–7.
31 J. Garcia-Anton, M. R. Axet, S. Jansat, K. Philippot, B. Chaudret, T. Pery, G. Buntkowsky and H. H. Limbach, *Angew. Chem., Int. Ed.*, 2008, **47**, 2074–2078.
32 T. Gutmann, I. del Rosal, B. Chaudret, R. Poteau, H. H. Limbach and G. Buntkowsky, *ChemPhysChem*, 2013, **14**, 3026–3033.
33 J. M. Asensio, D. Bouzouita, P. van Leeuwen and B. Chaudret, *Chem. Rev.*, 2020, **120**, 1042–1084.
34 L. M. Martinez-Prieto and B. Chaudret, *Acc. Chem. Res.*, 2018, **51**, 376–384.
35 C. Amiens, D. Ciuculescu-Pradines and K. Philippot, *Coord. Chem. Rev.*, 2016, **308**, 409–432.
36 P. Lara, K. Philippot and B. Chaudret, *ChemCatChem*, 2013, **5**, 28–45.
37 S. Mourdikoudis, R. M. Pallares and N. T. K. Thanh, *Nanoscale*, 2018, **10**, 12871–12934.
38 M. R. Axet and K. Philippot, *Chem. Rev.*, 2020, **120**, 1085–1145.
39 L. Huang, F. Zhang, W. Sun and X. Kang, *J. Colloid Interface Sci.*, 2021, **588**, 761–766.
40 T. Pery, K. Pelzer, G. Buntkowsky, K. Philippot, H. H. Limbach and B. Chaudret, *ChemPhysChem*, 2005, **6**, 605–607.
41 T. Gutmann, B. Walaszek, Y. Xu, M. Waechtler, I. del Rosal, A. Gruenberg, R. Poteau, R. Axet, G. Lavigne, B. Chaudret, H.-H. Limbach and G. Buntkowsky, *J. Am. Chem. Soc.*, 2010, **132**, 11759–11767.
42 B. Walaszek, A. Adamczyk, T. Pery, Y. Xu, T. Gutmann, N. d. S. Amadeu, S. Ulrich, H. Breitzke, H. M. Vieth, S. Sabo-Etienne, B. Chaudret, H.-H. Limbach and G. Buntkowsky, *J. Am. Chem. Soc.*, 2008, **130**, 17502–17508.
43 D. Bumüller, A.-S. Hehn, E. Waldt, R. Ahlrichs, M. M. Kappes and D. Schooss, *J. Phys. Chem. C*, 2017, **121**, 10645–10652.
44 I. del Rosal, T. Gutmann, L. Maron, F. Jolibois, B. Chaudret, B. Walaszek, H.-H. Limbach, R. Poteau and G. Buntkowsky, *Phys. Chem. Chem. Phys.*, 2009, **11**, 5657–5663.
45 I. del Rosal, T. Gutmann, B. Walaszek, I. C. Gerber, B. Chaudret, H.-H. Limbach, G. Buntkowsky and R. Poteau, *Phys. Chem. Chem. Phys.*, 2011, **13**, 20199–20207.
46 H. H. Limbach, T. Pery, N. Rothermel, B. Chaudret, T. Gutmann and G. Buntkowsky, *Phys. Chem. Chem. Phys.*, 2018, **20**, 10697–10712.
47 F. Applegath, M. D. Barnes and R. A. Franz, Preparation of Ureas, *US Pat.*, 2857430, 1958.

48 R. A. Franz and F. Applegath, *J. Org. Chem.*, 1961, **26**, 3304–3305.
49 A. R. Elman and V. I. Smirnov, *J. Environ. Sci. Eng.*, 2011, **5**, 1006–1012.
50 N. Rothermel, D. Bouzouita, T. Rother, I. de Rosal, S. Tricard, R. Poteau, T. Gutmann, B. Chaudret, H. H. Limbach and G. Buntkowsky, *ChemCatChem*, 2018, **10**, 4243–4247.
51 N. Rothermel, T. Röther, T. Ayvalı, L. M. Martínez-Prieto, K. Philippot, H.-H. Limbach, B. Chaudret, T. Gutmann and G. Buntkowsky, *ChemCatChem*, 2019, **11**, 1465–1471.
52 S. J. Opella and M. H. Frey, *J. Am. Chem. Soc.*, 1979, **101**, 5854–5856.
53 L. Cusinato, L. M. Martínez-Prieto, B. Chaudret, I. del Rosal and R. Poteau, *Nanoscale*, 2016, **8**, 10974–10992.
54 J. Creus, S. Drouet, S. Suriñach, P. Lecante, V. Collière, R. Poteau, K. Philippot, J. García-Antón and X. Sala, *ACS Catal.*, 2018, **8**, 11094–11102.
55 R. González-Gómez, L. Cusinato, C. Bijani, Y. Coppel, P. Lecante, C. Amiens, I. del Rosal, K. Philippot and R. Poteau, *Nanoscale*, 2019, **11**, 9392–9409.
56 V. Pfeifer, M. Certiat, D. Bouzouita, A. Palazzolo, S. Garcia-Argote, E. Marcon, D.-A. Buisson, P. Lesot, L. Maron, B. Chaudret, S. Tricard, I. del Rosal, R. Poteau, S. Feuillastre and G. Pieters, *Chem. – Eur. J.*, 2020, **26**, 4988–4996.
57 Á. Logadóttir and J. K. Nørskov, *J. Catal.*, 2003, **220**, 273–279.
58 L. M. Martínez-Prieto, I. Cano, A. Márquez, E. A. Baquero, S. Tricard, L. Cusinato, I. del Rosal, R. Poteau, Y. Coppel, K. Philippot, B. Chaudret, J. Cámpora and P. W. N. M. van Leeuwen, *Chem. Sci.*, 2017, **8**, 2931–2941.
59 T. Gutmann, E. Bonnefille, H. Breitzke, P.-J. Debouttiere, K. Philippot, R. Poteau, G. Buntkowsky and B. Chaudret, *Phys. Chem. Chem. Phys.*, 2013, **15**, 17383–17394.
60 T. Cendak, L. Sequeira, M. Sardo, A. Valente, M. L. Pinto and L. Mafra, *Chem. – Eur. J.*, 2018, **24**, 10136–10145.
61 D. T. Okamoto, S. L. Cooper and T. W. Root, *Macromolecules*, 1992, **25**, 1068–1073.
62 R. E. Taylor, A. D. Bacher and C. Dybowski, *J. Mol. Struct.*, 2007, **846**, 147–152.
63 A. E. Bennett, C. M. Rienstra, M. Auger, K. V. Lakshmi and R. G. Griffin, *J. Chem. Phys.*, 1995, **103**, 6951–6958.
64 P. R. Srinivasan and R. L. Lichter, *J. Magn. Reson.*, 1977, **28**, 227–234.
65 D. S. Wishart, C. G. Bigam, J. Yao, F. Abildgaard, H. J. Dyson, E. Oldfield, J. L. Markley and B. D. Sykes, *J. Biomol. NMR*, 1995, **6**, 135–140.
66 S. Hayashi and K. Hayamizu, *Bull. Chem. Soc. Jpn.*, 1991, **64**, 688–690.

